OPEN

Light: Science & Applications (2017) 6, e16218; doi:10.1038/lsa.2016.218
Official journal of the CIOMP 2047-7538/17
www.nature.com/lsa

ORIGINAL ARTICLE

Simple route toward efficient frequency conversion for generation of fully coherent supercontinua in the mid-IR and UV range

Ihar Babushkin[1,2], Ayhan Tajalli[1], Hakan Sayinc[3], Uwe Morgner[1,3,4], Günter Steinmeyer[2] and Ayhan Demircan[1,4]

Fiber supercontinua represent light sources of pivotal importance for a wide range of applications, ranging from optical communications to frequency metrology. Although spectra encompassing more than three octaves can be produced, the applicability of such spectra is strongly hampered due to coherence degradation during spectral broadening. Assuming pulse parameters at the cutting edge of currently available laser technology, we demonstrate the possibility of strongly coherent supercontinuum generation. In a fiber with two zero-dispersion wavelengths a higher-order soliton experiences a temporal breakdown, without any compression or splitting behavior, which leads to nearly complete conversion of input solitonic radiation into resonant nonsolitonic radiation in the dispersive wave regime. As the process is completely deterministic and shows little sensitivity to input noise, the resulting pulses appear to be compressible down to the sub-cycle level and may thus hold a new opportunity for direct generation of attosecond pulses in the visible to near ultraviolet wavelength range.
Light: Science & Applications (2017) **6,** e16218; doi:10.1038/lsa.2016.218; published online 10 February 2017

Keywords: attosecond pulses; optical solitons; supercontinuum; ultrashort pulses

INTRODUCTION

Generation of octave-spanning spectra is demanding at the relatively low excitation energies of oscillator sources. Such supercontinua have revolutionized frequency metrology with frequency combs in the visible to mid-infrared enabling ultrahigh-resolution spectroscopy[1–4]. Supercontinua encompassing more than three octaves have been produced, for example[5], in a ZBLAN photonic crystal fiber (PCF), spanning the range from 200 to 1750 nm. However, such ultrabroad spectral bandwidths come at the price of complex interaction scenarios, which cannot be easily adapted to generate short pulses anywhere close to the bandwidth limit of the supercontinuum. The production of such coherent pulses is highly appealing for applications that rely on the shortness of the pulse, for example, ultrafast spectroscopy. The common mechanism for supercontinuum generation in PCFs relies on a higher-order soliton breakup scenario via fission or modulation instability in fibers with a zero-dispersion wavelength (ZDW)[6–9], accompanied by the generation of Cherenkov-like radiation[10], which enables an efficient transfer of soliton energy into the normal dispersion regime[11]. This four-wave mixing-based process is often also called resonant radiation and is phase-matched for a wide wavelength range around one center wavelength. Group-velocity matching may additionally appear and further enhance the efficiency of the Cherenkov process. Although the scenario of soliton breakup is very efficient in terms of obtainable bandwidth of the supercontinuum, it is also highly susceptible to noise on the input pulse train. Even fluctuations on the quantum noise level suffice to produce substantial shot-to-shot variation of the output spectra. In practical terms, the output spectra lose their shot-to-shot coherence. Consequently, soliton fission (SF) supercontinua cannot be compressed into a train of short pulses anymore[6,7]. Using fibers with two ZDWs enables a simultaneous transfer of soliton energy to the two normal dispersion regions, both in the infrared as in the visible wavelength regime[12–14]. This dual transfer leads to a higher degree of coherence and further stabilization[15]. Such behavior has already been observed experimentally in pioneering works on SC generation in the 1550 nm telecommunication band[16–18]. In the latter studies, the critical dependence of the resulting spectra on the dispersion properties has already been recognized, but was not yet fully theoretically investigated at the time. The presence of a second ZDW has been reported to lead to a number of effects that are absent in single-ZDW fibers, for example, a modified spectral recoil phenomenon or the generation of coupled soliton pairs[13]. Nevertheless, the main underlying mechanism for supercontinuum generation is typically imposed by the standard soliton fission process, which has the same fundamental limits for coherence properties that inhibit the few- or even single-cycle pulse generation[19]. Somewhat unusual propagation dynamics have been observed experimentally[20] in fibers with a narrow anomalous dispersion region between two ZDWs. Here no soliton

[1]Institute of Quantum Optics, Leibniz Universität Hannover, 30167 Hanover, Germany; [2]Max Born Institute (MBI), 12489 Berlin, Germany; [3]Laser Zentrum Hannover e.V., 30419 Hanover, Germany and [4]Hanover Centre for Optical Technologies, 30167 Hanover, Germany
Correspondence: I Babushkin, Email: babushkin@iqo.uni-hannover.de
Received 1 March 2016; revised 1 September 2016; accepted 4 September 2016; accepted article preview online 6 September 2016

fission is observed for ultrashort input pulses and the energy in the anomalous dispersion region is completely depleted. Unfortunately, the resulting output spectral bandwidth does not appear significantly broader than the one resulting from self-phase modulation (SPM). Recently, some alternative mechanisms for supercontinuum generation have been discussed, which may enable to overcome the major shortcoming of the soliton breakup mechanism. For example, a fully coherent photonic chip-based optical frequency comb that spans 2/3 of an octave has been demonstrated, promising on-chip applications, that is, for frequency metrology[21]. The coherent broad spectral bandwidth is resulting from highly efficient transfer of energy to Cherenkov-like radiation. Going to the cutting edge of currently available laser technology, we predict a regime of soliton breakdown in fibers with two ZDWs. This process exploits the Cherenkov radiation with an extremely high efficiency. Using few-cycle input pulses with elevated pulse energies, the resulting breakdown is free of complicated pulse splitting behavior or compression and accomplishes a near-complete transfer of solitonic radiation into highly coherent octave-spanning spectra in the normal dispersion regime.

MATERIALS AND METHODS

For the investigations of the propagation dynamics, it is necessary to use a non-envelope variant of the nonlinear Schrödinger equation, which enables the description of propagation dynamics within a nonlinear optical waveguide for ultrashort pulses down to the sub-cycle regime. To this end, we numerically solve the unidirectional propagation equation[22,23] for the analytical signal $\mathscr{E}$, which is connected to optical field in frequency domain $E(z,\omega)$ by $\mathscr{E}(z,t) = 2\sum_{\omega>0} E(z,\omega)e^{-i\omega t}$. The resulting equation then reads

$$\partial_z \mathscr{E} + \hat{\beta}\mathscr{E} + \frac{n_2}{c}\partial_t\left(f_K|\mathscr{E}|^2\mathscr{E} + f_R\mathscr{E}\hat{h}|\mathscr{E}|^2\right)_+ = 0 \qquad (1)$$

where n_2 is the nonlinear refractive index (3×10^{-16} cm^2 W^{-1}), c is the speed of light in vacuum and $()_+$ denotes isolation of the positive frequency part by setting amplitudes at negative frequencies to zero. Operator $\hat{\beta}$ is defined in the frequency domain via multiplication to the propagation constant $\beta(\omega)$, and V is the velocity of the moving frame such that $\hat{\beta}\exp(-i\omega t) = -i[\beta(\omega) - \omega/V]\exp(-i\omega t)$. In our case, $\beta(\omega)$ is defined via the Padé approximation[24]. The parameters f_K and $f_R = 1 - f_K$ describe relative contributions of the Kerr and the Raman effect, respectively, and $\hat{h}$ denotes convolution with the Raman response function $\hat{h}|\mathscr{E}(z,t)|^2 = \int_0^\infty h(t')|\mathscr{E}(z,t-t')|^2 dt'$, where $h(t') = \exp(-t'/\tau_2)\sin(t'/\tau_1)(\tau_1^2+\tau_2^2)/\tau_1\tau_2^2$. The specific values of f_R and $\tau_{1,2}$ are assumed as 0.18, 12.2 and 32.0 fs, respectively. The velocity V is taken to be equal to that of the fundamental soliton for the corresponding frequency. A main advantage of this formalism is its inherent capability to correctly describe four-wave mixing processes between frequency components that are more than an octave apart. The resulting description of the optical field is equivalent to using the forward Maxwell equation[6], yet with the benefit of a clear separation from third harmonic generation, thus allowing to investigate the impact of the different effects independently. If the slowly varying envelope description is applied, Equation (1) reduces to the standard nonlinear Schrödinger equation, and the absolute magnitude of $\mathscr{E}(t, z)$ is same as that of the envelope. For numerical solution of Equation (1), we use a standard split-step method, with the implementation of the Runge–Kutta integration scheme for the nonlinear term and an adaptive step-size control in z. A standard de-aliasing procedure[25] has been employed throughout.

For our simulations, we consider a standard nonlinear fiber with two ZDWs, as it is commercially available (NL-PM 750). Dispersion properties are depicted in Figure 1a, where $\beta_1(\omega) = \beta'(\omega)$ and $\beta_2(\omega) = \beta''(\omega)$ are presented. The considered propagation lengths are much smaller than the inverse linear losses in the whole frequency range, that is, <0.1 dB cm^{-1}. Most notably, $\beta(\omega)$ displays two ZDWs at 0.79 and 1.26 μm with a relatively broad anomalous dispersion range (in contrast to the investigations in Ref 20). For the input pulse, we assume a high-order soliton of order N as given by $\mathscr{E}(t, z=0) = \mathscr{E}_0\mathrm{sech}(t/\tau)\exp(-i\omega_0 t)$, where τ is the pulse duration, ω_0 is the central frequency and $\mathscr{E}_0$ is the initial soliton amplitude related to N via $\mathscr{E}_0^2 = N^2|\beta_2|/(\gamma\tau^2)$. The number N plays important role in the soliton fission process[8,13]. We note that this initial condition does not correspond to any exact solution of Equation (1) (although it is an analytical solution of the simpler nonlinear Schrödinger equation). We further remark that under the assumption of arbitrary dispersion, Equation (1) generally possesses no analytical solution although it can be found for some dispersion profiles (and, alternatively, for other forms of the nonlinear term)[22,26,27].

RESULTS AND DISCUSSION

Let us first address the situation of a fiber with two ZDWs for the case of fairly conventional many-cycle input pulses, reflecting the usual well-known soliton fission process[26]. In this case, a higher-order soliton breakup is typically observed. Assuming equal pulse duration $\tau = 90$ fs and soliton order $N = 20$, but using three different input wavelengths between 800 and 1250 nm, one can observe different realizations of the soliton breakup process (Figure 1b–1g). For the input wavelength of 800 nm (Figure 1b and 1e), fundamental solitons split off the higher-order soliton one after the other during the propagation, which is known as SF. Choosing an input wavelength of 1250 nm, that is, close to the second ZDW (Figure 1d and 1g), the SF process leads to a formation of fundamental solitons with a higher group-velocity due to the negative β_3 coefficient for this wavelength. The solitons are ejected at the leading edge, which is accompanied by excitation of phase-matched radiation in the normal dispersion regime toward longer wavelengths. In the contrasting case of modulation instability (Figure 1c and 1f, input wavelength 1000 nm), fundamental solitons are created via breakup of the input pulse via Akhmediev breathers[28,29]. This case results in an even quicker degradation of the coherence[6,7,30,31]. In all cases, nonsolitonic Cherenkov radiation appears, and relatively long pulses of many cycles (>10) duration emerge.

Now going to shorter few-cycle input pulses, one expects that the concept of fundamental envelope solitons breaks down[32,33]. From a mathematical point of view, solitary solutions of pulse propagation equations are expected to either become unstable or exhibit singularities[34]. Practically, already in the two-cycle regime, formation of a rather unphysical cusp-like structure is theoretically predicted to form in the vicinity of the soliton peak. In reality, the formation of such discontinuous pulse shapes is prevented by the actual dispersion properties of the medium. Consequently, the neglected spectral dispersion of linear and nonlinear properties determines the shortest obtainable possible pulse duration and limits the largest possible peak power. However, little is known about few-cycle higher-order solitons although such pulses are nowadays experimentally accessible. Especially, there should be a strong impact of this limiting phenomenon on the well-known supercontinuum generation process by soliton fission.

Starting at a pulse duration of about 10 cycles and decreasing the duration further, we see increasingly strong deviations from the well-known breakup scenarios, with solitons eventually dying out at about six cycles duration. It is important to note, that we investigate the propagation dynamics in the few-cycle regime for similar soliton

doi:10.1038/lsa.2016.218

orders ($N=10$ and below), to underline that the standard soliton fission process is not scalable into the few-cycle soliton regime. In our new scenario, the high-order soliton is rapidly annihilated on a scale of just hundreds of micrometers of propagation, without the ejection of any fundamental soliton. We do not observe any soliton compression, the typical first step of the higher-order soliton propagation. There is also neither any increase of peak intensity nor decrease of pulse width. In contrast, the amplitude of the soliton experiences tremendous decrease on the extremely short propagation scale. These new dynamics are shown in Figure 2 for the case of N=10, τ=10 fs and λ=1000 nm. In the course of the catastrophic collapse in the time domain (Figure 2a and 2b), the spectrum also broadens dramatically (Figure 2c and 2d). This disruptive broadening is governed by the combined action of SPM, shock formation due to self-steepening, as well as emission of phase-matched Cherenkov radiation. Especially, the impact of the shock formations appears to have an important role for the significant spectral broadening. There is no soliton fission and the output spectrum results in a complete depletion of the anomalous dispersion regime. This behavior is similar to the experimental observation in Ref. 20, although in our case the spectral broadening is much stronger than would be allowed by SPM.

An increase of the efficiency of the energy transfer to dispersive waves for ultrashort pulses pumped in the anomalous dispersion regime has been observed experimentally in a fiber with one ZDW. In Refs 35, 36 conversion efficiency (up to 40%) and broad bandwidth for the isolated Cherenkov radiation are reported, where the typical frequency up-conversion process has been exploited by employing pump pulses in the few-cycle regime. In the course of the implosion-

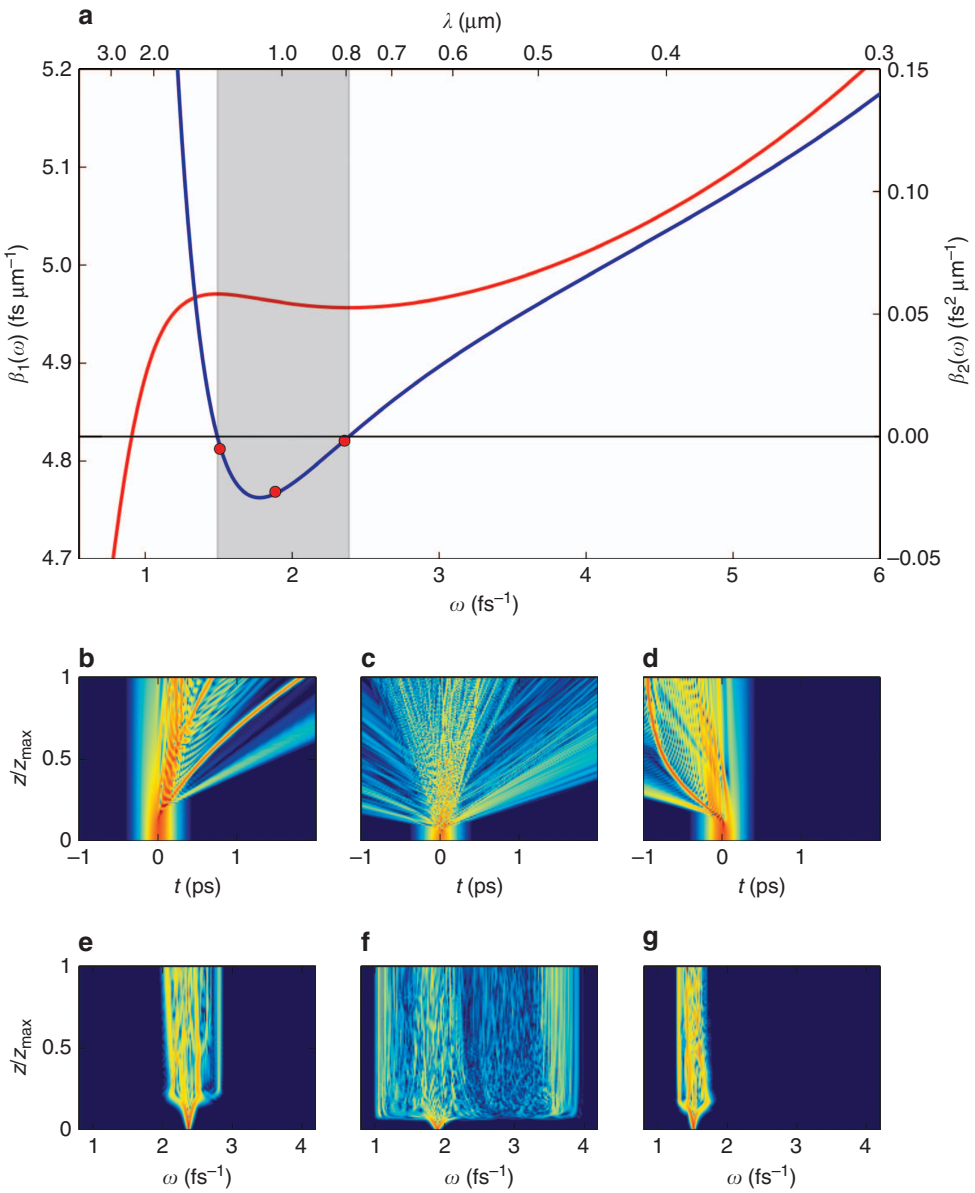

Figure 1 Typical scenarios of high-order soliton breakup, assuming NL-PM-750 photonic crystal fiber with two zero-dispersion wavelengths throughout. (**a**) Propagation constant $\beta_1(\omega)$ (red curve) and group-velocity dispersion $\beta_2(\omega)$ (blue curve). (**b**–**d**) Temporal pulse evolution. (**e**–**g**) Spectral evolution. (**b**, **e**) Soliton fission, $\tau=90$ fs, $N=20$ and $\lambda_0=800$ nm. (**d**, **g**) Same as in **b** and **e**, but $\lambda_0=1250$ nm in a range where the β_3 component changed sign. (**c**, **f**) Modulation instability, $\lambda_0=1000$ nm with $\beta_3\approx0$. The intensity in **b**–**g** is in logarithmic scale, the colorbar is presented in Figure 2c.

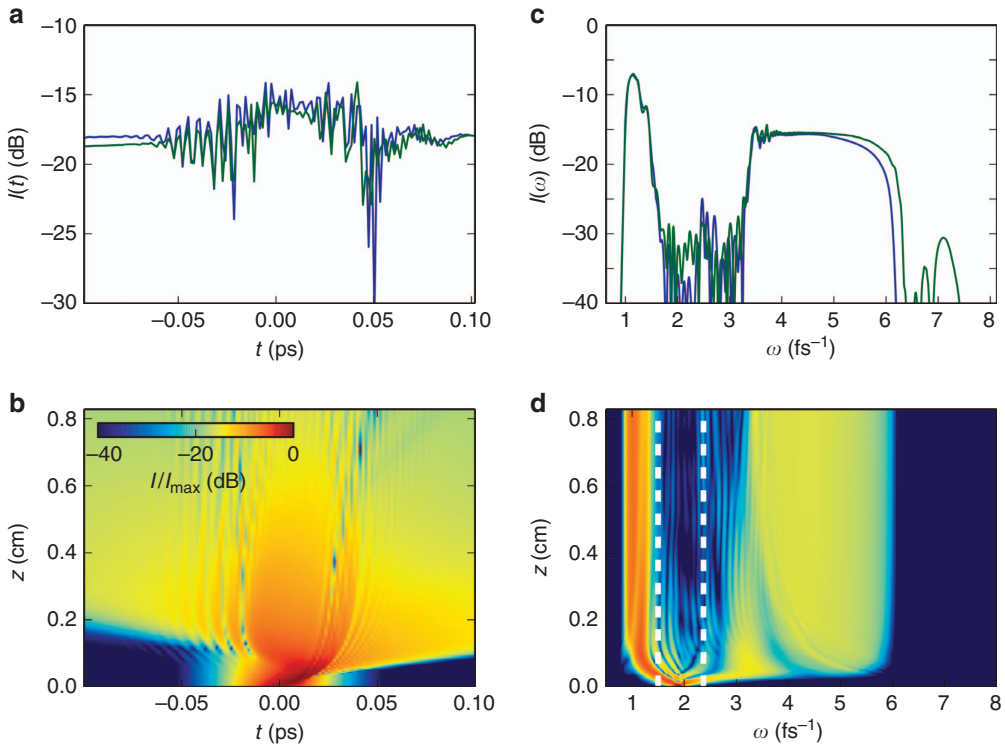

Figure 2 High-order soliton breakdown in (**a**, **b**) time domain and (**c**, **d**) frequency domain for an input soliton with duration of 10 fs, soliton order 10 and input wavelength 1000 nm. The propagation dynamics resulting from Equation (1) are shown in **b** and **d**. The corresponding output at the end of the fiber is shown in **a** and **c** (blue lines). The green lines represent the output corresponding to the dynamics with the inclusion of further higher-order effects (see text). The soliton is very quickly steepened and then completely converted into nonsolitonic radiation, with no remaining radiation in the solitonic (anomalous dispersion) range. Dashed white lines in **d** indicate the boundaries of the anomalous dispersion range. The output corresponds to the dispersive waves with bandwidths of low- and high-frequency parts being nearly an octave long. The color scale for **d** coincides with the one for **b**.

like behavior observed here, nearly all energy is pushed out of the anomalous dispersion range. Subsequently, the pulse starts to temporally broaden quickly because of joint action of nonlinearity and normal dispersion. Finally, after a few millimeters of propagation, the peak intensity decreases to a level where nonlinearities become negligible. Figure 2a and 2c shows the temporal and spectral profile at the end of the fiber, respectively. The blue lines represent the results obtained directly with Equation (1). It is worth noting that the soliton breakdown appears to be fairly general and does not depend critically on particular effects in the propagation equation apart from generic dispersion and a Kerr-type nonlinearity. In particular, we were able to reproduce the same behavior when excluding the Raman term. In fact, omission of the Raman effect leads to even broader spectra. As the soliton disappears very fast, there is no soliton-self frequency shift[37], which can be accounted for a modified recoil effect, and the Raman effect appears as a marginal perturbation. We also performed test calculations with the other variant of the propagation equation, namely unidirectional equation including harmonic generation and dispersion in the nonlinear term to all orders (green lines in Figure 2a and 2c)[8,38,39], which reveals only marginal effect on the overall observed process. Furthermore, robustness of the whole process is further confirmed by simulation with initial pulses that deviate from ideal higher-order soliton shapes.

Figure 3 shows the detailed evolution of the soliton implosion for the first few hundreds of micrometers for $\tau = 20$ fs and $N = 20$. The initial pulse immediately experiences steepening at its leading edge, and a shock front is formed (red line in Figure 3a). The shock zone is only ~ 250 attoseconds long (in contrast to the pulse duration). These findings indicate a prevalent role of Kerr-induced self-steepening effects in the pulse shaping dynamics. The shock front formation is accompanied by rapid spectral broadening as shown in Figure 3b. At the onset of this process, most of the pulse energy is already transferred towards outside the initial soliton wavelength range. Some part of the energy goes to the low-frequency part of the spectrum, whereas another part is transferred into the visible range. This process reaches remarkable efficiency in a fiber with two dispersion zeros, as such a refractive index profile enables phase-matching on both sides of the anomalous dispersion regime, similar to the simultaneous transfer of energy across both sides of the anomalous dispersion regime in the standard supercontinuum generation process[40]. A further characteristic of the supercontinuum demonstrated here is an early stagnation of the spectral broadening process, followed by static propagation without further changes of the spectral properties, indicating that no further FWM or other interaction processes have an important role.

It appears illustrative to track changes of soliton behavior with increasing soliton order (Figure 4). For instance, consider the blue curve corresponding to the case $\tau = 5$ fs. At low intensities ($N \approx 1$), stable soliton propagation takes place, which is only slightly affected by the Raman effect. No significant energy transfer to a dispersive wave takes place, which also holds for soliton numbers up to $N \approx 2$. Beyond this value, a sharp transition to another regime appears, and an annihilation of the soliton takes over without any stable soliton propagation anymore. The exact transition point critically depends on pulse duration. At $\tau = 2.5$ fs (1.5-cycle pulse), for example, the transition already appears at $N = 2$, whereas in case of longer solitons (30 fs duration), annihilation only sets in for $N \sim 10$. For even longer

doi:10.1038/lsa.2016.218

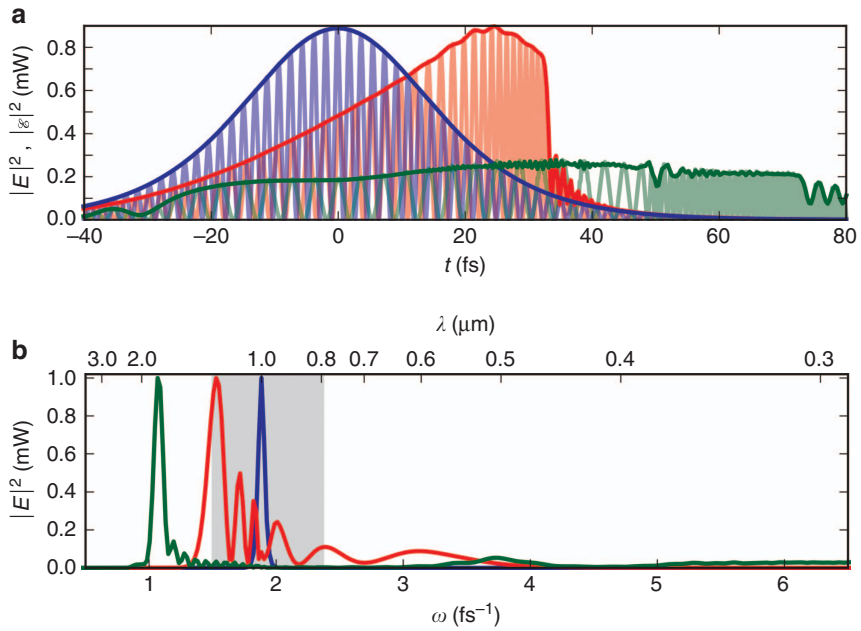

Figure 3 (**a**, **b**) Detailed representation of the soliton implosion process in time **a** and frequency **b** domain for $\tau = 20$ fs, $N = 20$. Anomalous dispersion range in **b** is indicated by a shaded region. Fast oscillating lines correspond to the square of electric field E^2, whereas the slow envelope-like lines to $|\mathscr{E}|^2$. The field at $z = 0$ (blue lines), directly at the point of shock formation (red lines) and immediately afterwards (green lines) is plotted. The duration of the steepest shock phase is as small as ~250 attoseconds.

pulses, the full soliton breakdown with complete energy removal from the anomalous dispersion regime does not appear anymore at realistic input pulse energies. As one can see from Figure 4a, the soliton behavior before and after the breakdown threshold is different in another important respect. Below the threshold, the higher-order soliton shows typical recompression behavior, accompanied with the decrease of the pulse duration and increase of the peak intensity (Figure 4a, dashed line). Cherenkov radiation is created but there is still enough energy in the anomalous range, which also does not disappear with further propagation (Figure 4c and 4e). This is not anymore the case for the pulses above the breakdown threshold as shown in Figure 4d and 4f. In this case, no pulse recompression takes place at all (see Figure 4a, solid line, as well as Figure 3).

We have to point out here again that the complete depletion of the energy in the anomalous dispersion regime appears during an extremely short propagation distance of few hundreds micrometers. The significant spectral broadening appears therefore as an implosion-like behavior. The resulting supercontinuum spectra on both sides are generated on much shorter distances than in the standard soliton fission process.

One of the main important features of the soliton annihilation process is its inherent capability of producing completely coherent and compressible spectra. Other than soliton fission, the process is absolutely deterministic and does not critically depend on input noise. Propagation dynamics in the normal dispersion regime is generally known to exhibit a low sensitivity to quantum noise[6,7], thus making it preferable to immediately transfer the whole energy into this region. Figure 5a and 5b displays the spectrum of one-shot at the end of the fiber of the low- and high-frequency parts, together with the corresponding spectral phase for the case $\tau = 5$ fs, $N = 8$. The spectrum is extremely smooth over the entire range, in contrast to super-continua typically generated by soliton fission. The phase does not exhibit any strong irregularities, an important characteristic to go beyond the fundamental limitations for few-cycle pulse generation from standard supercontinuum spectra[19]. Compressibility of the spectra therefore appears to be fairly straightforward. To demonstrate the superior coherence properties of our scheme (see Figure 5a and 5b, green lines), we calculate the modulus of the complex degree of first-order coherence[41], $|g(\omega)|$ as a measure for the SC phase stability $g(\omega) = <\mathscr{E}_i(\omega)\mathscr{E}_j(\omega)>_{i\neq j} / <|\mathscr{E}(\omega)|^2>$, where the angular brackets denote an ensemble average over 410 pairs of SC spectra. These spectra are independently numerically generated by using different quantum-limited shot noise seeds. In the numerator the average is made over all possible pairs $\{\mathscr{E}_i, \mathscr{E}_j\}$ in the ensemble, excluding $i = j$. In these simulations we did not observe indications for pulse splitting or strong irregularities on the output pulses, see Figure 5c and 5d. For further demonstration, we separately simulate compression of either the low-frequency or the high-frequency part of the spectrum, as obtained for input pulses with $\tau = 5$ fs and $N = 8$. The corresponding output dispersive waves are shown in Figure 5e and 5f, respectively. As the pulses are created at a very early stage of the propagation dynamics in the fiber and linearly disperse with successive propagation, the resulting nonlinear and linear phase contributions on the pulses can be easily compensated for by prism pairs or dispersion shapers, provided only that the propagation length in the fiber is kept at a minimum. The high-frequency part of the spectrum appears from 315 to 787 nm. This part of the spectrum is compressed into a 2.8-nJ sub-cycle pulse with a FWHM of 0.32 fs, as shown in Figure 5f. In addition, the low-frequency part of the spectrum from 1260 to 3780 nm is separately compressed to a 2.6-nJ pulse with a FWHM duration of 16 fs, that is, encompassing only about 1.5 oscillation cycles (Figure 5e).

For the complete conversion of soliton radiation into octave-spanning Cherenkov radiation spectra, one requires pulse energies in excess of 5 nJ at few-cycle pulse duration to be launched into a photonic crystal fiber. These requirements do not seem to lie much above commercially available two-cycle Ti:sapphire oscillators offering

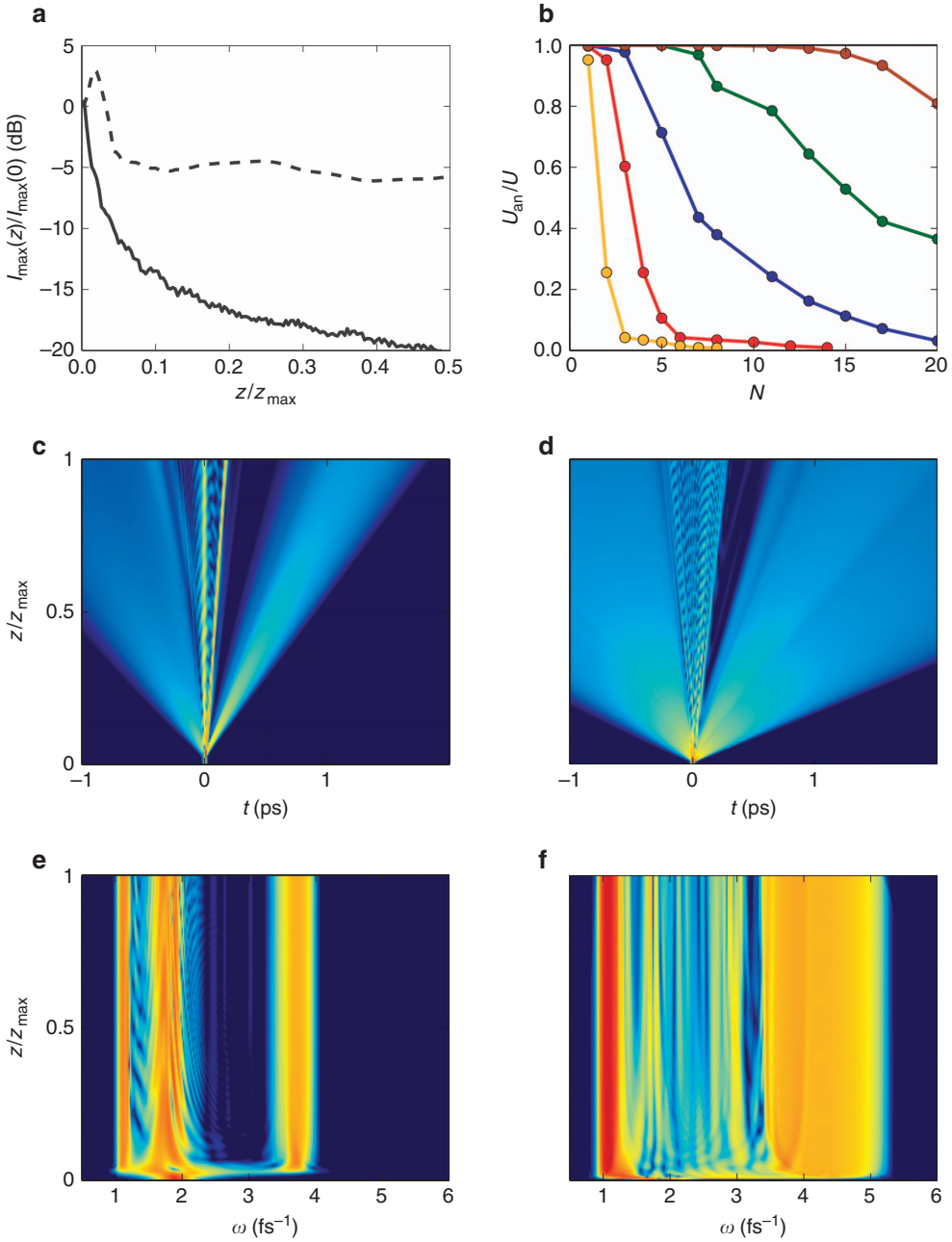

Figure 4 Transition from high-order soliton breakup via SF or MI to soliton breakdown via implosion with increasing soliton number N. (**a**) Peak intensity in dependence on propagation distance for a soliton just below threshold of breakdown ($N=2$; dashed line), and immediately above threshold ($N=5$; solid line) for $\tau=5$ fs assuming propagation distance $z_{max}=6$ cm. (**b**) Dependence of the part of the pulse energy in the anomalous dispersion region U_{an} on the whole pulse energy U for $\tau=2.5$ fs, $\lambda_0=1000$ nm (orange line), $\tau=5$ fs, $\lambda_0=1000$ nm (red line), $\tau=30$ fs, $\lambda_0=1000$ nm (blue line), $\tau=90$ fs, $\lambda_0=1000$ nm (green line) and $\tau=90$ fs, $\lambda_0=800$ nm (brown line). Lines depict linear interpolation between the calculated points shown by circles of corresponding color. (**c**–**f**) Propagation dynamics: temporal pulse dynamics (**c**, **d**), frequency domain dynamics (**e**, **f**) for soliton just below threshold of breakdown for $N=2$ (**c**, **e**) and immediately above threshold ($N=5$) (**d**, **f**) for $\tau=5$ fs. The intensity in **c**–**f** is in logarithmic scale, the colorbar is presented in Figure 2c.

up to 3 nJ at the oscillator output, but the associated non-Gaussian beam profiles typically only enable coupling of a fraction of the available energy into the fiber. Low-repetition rate sources exist that can easily offer sufficient pulse energy even at 10% coupling efficiencies, yet at the price of about five times longer pulse duration. In either case, parameters are about one order of magnitude away from inducing a soliton breakdown inside the fiber. Another constraint arises as input peak powers of nearly 10^{14} W cm^{-2} (for few-cycle pulses) are expected to generate catastrophic optical damage at the input face of fused-silica-based photonic crystal fibers. Experimental verification of the described soliton breakdown scenario requires either a way of increasing coupling efficiencies of few-cycle pulses into the fiber or suitable dispersion management, such that catastrophic damage is avoided at the fiber input. Finally, compression of such broadband pulses requires a suitable compressor scheme. Avoiding overlapping orders of grating-based schemes, a prism-based compressor[42] offers sufficient spectral resolution together with coverage beyond the optical octave. We further note that even at energies

doi:10.1038/lsa.2016.218

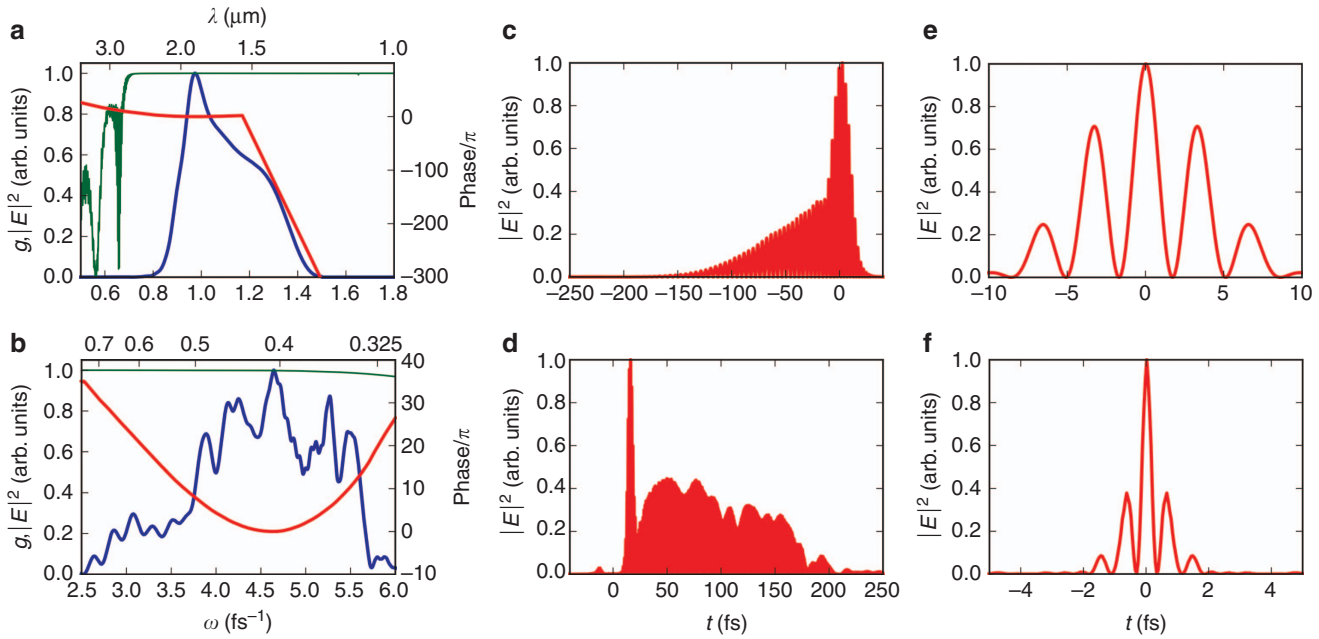

Figure 5 Compressible dispersive waves. (**a**, **b**) The low- and high-frequency spectral parts (blue lines) of one-shot at the fiber output $z=0.8$ cm for $\tau=5$ fs and $N=8$, corresponding spectral phase (red lines), and the modulus of the complex degree of first-order coherence $|g(\omega)|$ (green lines) are shown. The corresponding pulses in time domain in (**c**) and (**d**) and their fully compressed versions in (**e**) and (**f**) are presented. Resulting compressed pulses contain 2.6 and 2.8 nJ, respectively, and exhibit a FWHM duration of 16 fs and 320 attoseconds, respectively.

lower than needed for soliton breakdown, clear precursors of this regime have been reported, in particular, a significant increase of energy transfer to nonsolitonic radiation[35,36]. Those precursors were experimentally observed, yet in a fiber with only one ZDW. Furthermore, the isolated depletion of soliton energy between two zero ZDWs, yet without broadband supercontinuum generation, has been observed experimentally for narrow anomalous dispersion[20]. Our results show that this scenario becomes much more pronounced if one goes into the few-cycle regime.

In closing, let us emphasize that the concept of soliton implosion is not restricted to material and pulse parameters used in our investigation. In fact, it can be readily transferred to other fibers with two ZDWs. One particular promising candidate appears to be a solid-core ZBLAN fiber, which we expect to widen the obtainable supercontinuum width significantly because of stronger nonlinearity and higher achievable dispersion enabling few-cycle solitons at lower intensities.

CONCLUSIONS

We numerically explored a new regime of supercontinuum generation in optical fibers, enabling the process of soliton breakdown, which coherently converts solitonic radiation nearly completely into dispersive radiation. The resulting supercontinua appear fully compressible, both as they maintain inter-pulse coherence as well as they do not result in overly complicated spectral phase modulations. Soliton annihilation critically relies on a combination of short input pulse duration and elevated input pulse energies, which seem to be slightly beyond the limits of currently available off-the-shelf technology. Moreover, our concept only lives to its full beauty for particular resonance conditions that are only available in fibers with two dispersion zeros. Given the demonstrated advantages of this dynamics, we nevertheless believe that our work can be particularly stimulating for experimentalists working in this field. Such broad spectra will be attractive for creation of ultrashort pulses beyond the femtosecond duration limit as well as broadband frequency combs.

CONFLICT OF INTEREST

The authors declare no conflict of interest.

ACKNOWLEDGEMENTS

We gratefully acknowledge support by the DFG (projects BA 4156/4-1, MO 850/19-1) and Nieders. Vorab (project ZN3061).

1 Udem T, Reichert J, Haensch T, Kourogi M. Accuracy of optical frequency comb generators and optical frequency interval divider chains. *Opt Lett* 1998; **23**: 1387–1389.
2 Jones DJ, Diddams SA, Ranka JK, Stentz A, Windeler RS *et al*. Carrier-envelope phase control of femtosecond mode-locked lasers and direct optical frequency synthesis. *Science* 2000; **288**: 635–639.
3 Brumer PW, Shapiro M. *Principles of the Quantum Control of Molecular Processes*. London: Wiley-Interscience; 2003.
4 Krauss G, Lohss S, Hanke T, Sell A, Eggert S *et al*. Synthesis of a single cycle of light with compact erbium-doped fibre technology. *Nat Photonics* 2010; **4**: 33–36.
5 Jiang X, Joly NY, Finger MA, Babic F, Wong GKL *et al*. Deep-ultraviolet to mid-infrared supercontinuum generated in solid-core ZBLAN photonic crystal fibre. *Nat Photonics* 2015; **9**: 133–139.
6 Dudley JM, Genty G, Coen S. Supercontinuum generation in photonic crystal fiber. *Rev Mod Phys* 2006; **78**: 1135–1184.
7 Dudley JM, Taylor JR. Ten years of nonlinear optics in photonic crystal fibre. *Nat Photonics* 2009; **3**: 85–90.
8 Husakou AV, Herrmann J. Supercontinuum generation of higher-order solitons by fission in photonic crystal fibers. *Phys Rev Lett* 2001; **87**: 203901.
9 Cristiani I, Tediosi R, Tartara L, Degiorgio V. Dispersive wave generation by solitons in microstructured optical fibers. *Opt Express* 2004; **12**: 124–135.
10 Akhmediev N, Karlsson M. Cherenkov radiation emitted by solitons in optical fibers. *Phys Rev A* 1995; **51**: 2602–2607.
11 Skryabin DV, Luan F, Knight JC, Russell PStJ. Soliton self-frequency shift cancellation in photonic crystal fibers. *Science* 2003; **301**: 1705–1708.
12 Gaeta AL. Nonlinear propagation and continuum generation in microstructured optical fibers. *Opt Lett* 2002; **27**: 924–926.

13 Frosz MH, Falk P, Bang O. The role of the second zero-dispersion wavelength in generation of supercontinua and bright-bright soliton-pairs across the zero-dispersion wavelength. *Opt Express* 2005; **13**: 6181–6192.
14 Hilligsøe KM, Paulsen HN, Thøgersen J, Keiding SR, Larsen JJ. Initial steps of supercontinuum generation in photonic crystal fibers. *J Opt Soc Am B* 2003; **20**: 1887–1893.
15 Genty G, Coen S, Dudley JM. Fiber supercontinuum sources (invited). *J Opt Soc Am B* 2007; **24**: 1771–1785.
16 Morioka T, Mori K, Kawanishi S, Saruwatari M. Nearly penalty-free, <4 ps supercontinuum Gbit/s pulse generation over 1535-1560 nm. *Electron Lett* 1994; **30**: 790–791.
17 Mori K, Takara H, Kawanishi S, Saruwatari M, Morioka T. Flatly broadened supercontinuum spectrum generated in a dispersion decreasing fibre with convex dispersion profile. *Electron Lett* 1997; **33**: 1806–1808.
18 Collings BC, Mitchell ML, Boivin L, Knox WH. A 1021 channel WDM system. *IEEE Photonics Technol Lett* 2000; **12**: 906–908.
19 Dudley JM, Coen S. Fundamental limits to few-cycle pulse generation from compression of supercontinuum spectra generated in photonic crystal fiber. *Opt Express* 2004; **12**: 2423–2428.
20 Hilligsøe KM, Andersen TV, Paulsen HN, Nielsen CK, Mølmer K *et al*. Supercontinuum generation in a photonic crystal fiber with two zero dispersion wavelengths. *Opt Express* 2004; **12**: 1045–1054.
21 Brasch V, Geiselmann M, Herr T, Lihachev G, Pfeiffer MHP *et al*. Photonic chip–based optical frequency comb using soliton Cherenkov radiation. *Science* 2016; **351**: 357–360.
22 Amiranashvili S, Demircan A. Hamiltonian structure of propagation equations for ultrashort optical pulses. *Phys Rev A* 2010; **82**: 013812.
23 Amiranashvili S, Demircan A. Ultrashort optical pulse propagation in terms of analytic signal. *Adv Opt Technol* 2011; **2011**: 989515.
24 Amiranashvili S, Bandelow U, Mielke A. Padé approximant for refractive index and nonlocal envelope equations. *Opt Commun* 2010; **283**: 480–485.
25 Canuto C, Hussaini MY, Quarteroni A, Zang TA. *Spectral Methods in Fluid Dynamics*. Berlin: Springer; 1988.
26 Leblond H, Mihalache D. Models of few optical cycle solitons beyond the slowly varying envelope approximation. *Phys Rep* 2013; **523**: 61–126.
27 Kozlov SA, Sazonov SV. Nonlinear propagation of optical pulses of a few oscillations duration in dielectric media. *J Exp Theor Phys* 1997; **84**: 221–228.
28 Akhmediev N, Korneev VI. Modulation instability and periodic solutions of the nonlinear Schrödinger equation. *Theor Math Phys* 1986; **69**: 1089–1093.
29 Mahnke C, Mitschke F. Possibility of an Akhmediev breather decaying into solitons. *Phys Rev A* 2012; **85**: 033808.
30 Demircan A, Bandelow U. Analysis of the interplay between soliton fission and modulation instability in supercontinuum generation. *Appl Phys B* 2007; **86**: 31–39.
31 Demircan A, Amiranashvili S, Brée C, Steinmeyer G. Compressible octave spanning supercontinuum generation by two-pulse collisions. *Phys Rev Lett* 2013; **110**: 233901.
32 Amiranashvili S, Bandelow U, Akhmediev N. Dispersion of nonlinear group velocity determines shortest envelope solitons. *Phys Rev A* 2011; **84**: 043834.
33 Amiranashvili S, Bandelow U, Akhmediev N. Spectral properties of limiting solitons in optical fibers. *Opt Express* 2014; **22**: 30251–30256.
34 Sakovich A, Sakovich S. Solitary wave solutions of the short pulse equation. *J Phys A: Math Gene* 2006; **39**: L361–L367.
35 Chang GQ, Chen LJ, Kärtner FX. Highly efficient Cherenkov radiation in photonic crystal fibers for broadband visible wavelength generation. *Opt Lett* 2010; **35**: 2361–2363.
36 Chang GQ, Chen LJ, Kärtner FX. Fiber-optic Cherenkov radiation in the few-cycle regime. *Opt Express* 2011; **19**: 6635–6647.
37 Mitschke FM, Mollenauer LF. Discovery of the soliton self-frequency shift. *Opt Lett* 1986; **11**: 659–661.
38 Babushkin I, Herrmann J. High energy sub-10 fs pulse generation in vacuum ultraviolet using chirped four wave mixing in hollow waveguides. *Opt Express* 2008; **16**: 17774–17779.
39 Babushkin IV, Noack F, Herrmann J. Generation of sub-5 fs pulses in vacuum ultraviolet using four-wave frequency mixing in hollow waveguides. *Opt Lett* 2008; **33**: 938–940.
40 Genty G, Lehtonen M, Ludvigsen H, Kaivola M. Enhanced bandwidth of supercontinuum generated in microstructured fibers. *Opt Express* 2004; **12**: 3471–3480.
41 Genty G, Surakka M, Turunen J, Friberg AT. Complete characterization of supercontinuum coherence. *J Opt Soc Am B* 2011; **28**: 2301–2309.
42 Binhammer T, Rittweger E, Ell R, Kärtner FX, Morgner U. Prism-based pulse shaper for octave spanning spectra. *IEEE J Quant Electron* 2005; **41**: 1552–1557.